SYMBOLIC DYNAMICS IN THE PLANAR THREE-BODY PROBLEM

RICHARD MOECKEL

1. Introduction

1.1. **Description of Results.** Consider the motion of three point masses, m_1, m_2, m_3, in a plane under the influence of their mutual gravitational attraction. This motion can be described by a Hamiltonian dynamical system of three degrees of freedom. In this paper, symbolic dynamical methods will be used to prove the existence of solutions of this Hamiltonian system which exhibit certain interesting qualitative behaviors. The types of behavior considered are shown in figure 1.

The first kind of behavior is a close approach to triple collision. In 1767, Euler found simple solutions of the three-body problem which featured triple collisions in both forward and backward time [10]. He found that if the three bodies are arranged in a line and if the spacing between them is chosen in exactly the right way, then if they are released with zero initial velocity they will collapse homothetically to a triple collision. The spacing depends on the ordering of the masses along the line and on the ratios of the masses. Up to rotation and scaling, there are just three such special configurations, one for each rotationally distinct ordering of the masses along the line. Lagrange found that the same motion occurs if the particles are arranged in an equilateral triangle (independently of the masses). Up to rotation and scaling there are two equilateral configurations distinguished by whether the masses occur in counterclockwise or in clockwise order around the triangle. The five special configurations are called *central configurations*. Each of the central configurations also gives rise to a family of periodic solutions with nonzero angular momentum; these are shown in figure 1. Along such a solution, each mass describes a Keplerian elliptical orbit. The triangle formed by the three masses rotates and changes size but always remains similar to the original central configuration. When the angular momentum is small, the ellipses are very eccentric and so the masses pass close to triple collision. As will be seen, these special periodic solutions are by no means the only interesting near-collision solutions. One may ask what would happen if the initial conditions leading to one of the Lagrangian or Eulerian periodic solutions were to be perturbed slightly. The solutions constructed below show that a wide variety of behaviors is possible.

The second kind of qualitative behavior considered here is an excursion "near infinity". In contrast to the two-body problem, the conservation of energy places no restriction on the size of the triangle formed by the three masses. The phrase "near infinity" means that the largest edge of this triangle is large. In the negative energy

Date: February 2, 2007 (Preliminary Version).
2000 *Mathematics Subject Classification.* 70F10, 70F15, 37N05, 76Bxx.
Key words and phrases. Celestial mechanics.
Research supported by NSF grant DMS 0500443.

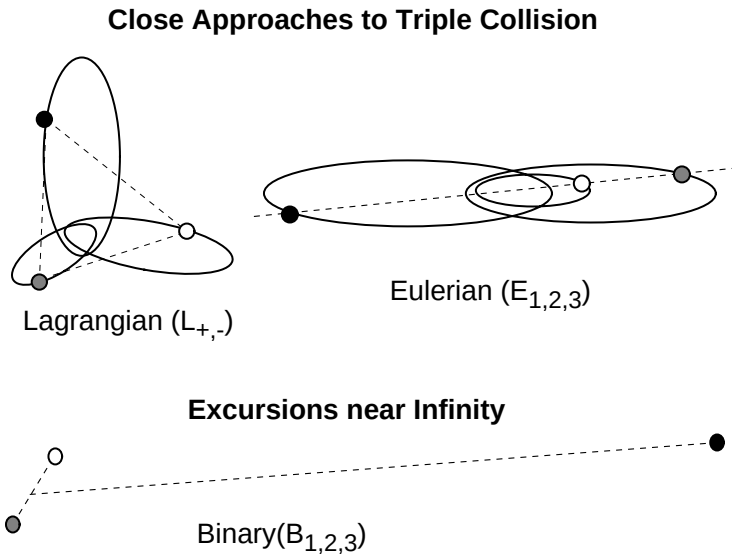

FIGURE 1. Kinds of Behavior Considered

case considered here, this can only happen as in figure 1; two of the masses remain a bounded distance apart while the other mass recedes. In this situation, the two nearby masses will be called the *binary* and the other mass will be called simply the *third mass*. The solutions near infinity can be classified according to the behavior of the distance between the third mass and the center of mass of the binary (the long dotted line in figure 1). This quantity will be called the *separation* and its derivative the *velocity of separation*. If the velocity of separation is large enough, the separation will tend to infinity. The velocity of separation approaches a limit. If this limit is positive, the solution is called *hyperbolic*; if it is zero, the solution is called *parabolic*. On the other hand the velocity of separation may be inadequate to overcome the attraction of the binary and the third mass. In this case, the separation reaches a maximum and the binary and the third mass approach one another. Such a solution is called *elliptic*.

Some terminology has been introduced to describe solutions which feature such excursions near infinity. An *escape orbit* is a solution for which the separation between the binary and the third mass is bounded in backward time but tends to infinity in forward time. Similarly, on a *capture orbit* the separation is bounded in forward time but tends to infinity in backward time. A solution for which the separation becomes infinite in both time directions (possibly with different third masses) is called a *scattering solution*. Finally, a solution which exhibits an infinite sequence of elliptic excursions near infinity with the sequence of maximum separations tending to infinity is called an *oscillating solution*. Of course these are just definitions and it is not immediately clear that solutions of this type actually exist. One of the main goals of this paper is to show that all of these behaviors occur.

Symbolic dynamics will be used to prove the existence of an invariant set for the planar three-body problem which contains:

- the Eulerian and Lagrangian periodic solutions
- infinitely many other periodic solutions exhibiting close approaches to triple collision
- homoclinic and heteroclinic orbits connecting these periodic solutions
- capture, escape and oscillating solutions which are heteroclinic between infinity and any of the bounded near-collision orbits in the invariant set
- scattering solutions with arbitrary third masses (possibly different as $t \to \pm\infty$) and with arbitrarily long bounded parts

To introduce symbolic dynamics, one has to construct a collection of "boxes" or "windows" and flow-defined Poincaré mappings which stretch the boxes across one another in an appropriate way. As it happens, the planar problem with fixed energy and angular momentum can be reduced to a dynamical system on a five-dimensional manifold. The boxes will be four-dimensional cubes transverse to the flow. Once the boxes and Poincaré mappings have been constructed, the existence of a large invariant set follows immediately: given any sequence of boxes such that each pair of successive boxes is connected by a Poincaré mapping, the exist a solution of the planar three-body problem which *realizes the sequence* in the sense that the solution passes through the boxes in the given order. The behavior between boxes is implicitly described by the Poincaré mappings.

The boxes and Poincaré mappings employed are shown in figure 2. This figure shows a directed graph with eight vertices and numerous edges. The vertices represent boxes which will be used in the construction and the edges represent Poincaré mappings connecting the boxes. Sequences of boxes and mappings determine paths in the graph. The labelling of the vertices corresponds to that in figure 1. The vertices labelled $L_\pm$ represent small four-dimensional boxes in a manifold of constant energy and angular momentum transverse to the Lagrangian periodic solutions. Thus any solution in the invariant set which corresponds to a path in the graph passing through one of these vertices must pass through such a box and therefore, by continuity with respect to initial conditions, will behave for a while like one of the highly eccentric Lagrangian periodic solutions. The vertices labelled E_j represent boxes constructed close to (but not intersecting) the other three classical periodic solutions. A solution represented by a path in the graph containing such a vertex will behave like one of the eccentric collinear periodic orbits while the bodies are far from their closest approach. Then near their close encounter, they revert to a nearly equilateral shape. On the other hand, the vertices B_j represent boxes near infinity with the subscript indicating the third mass. These boxes will be constructed in such a way that a solution corresponding to a path in the graph which passes though such a vertex many times in succession will feature a long excursion near infinity, that is, the maximum separation will be large. Moreover, if the path cycles through such a vertex indefinitely, the corresponding solution will tend parabolically to infinity. Thus by choosing appropriate paths in the graph one can produce all of the different qualitative behaviors listed above (and many more).

More information about the detailed behavior of the solutions in the invariant set can be inferred from the way that the Poincaré maps are defined. In particular, the arrows connecting Euler and Lagrange vertices in figure 2 represent a single close approach to triple collision. Thus if a path contains such an arrow, the corresponding solution approaches triple collision near one central configuration, avoids collision, and emerges near another central configuration.

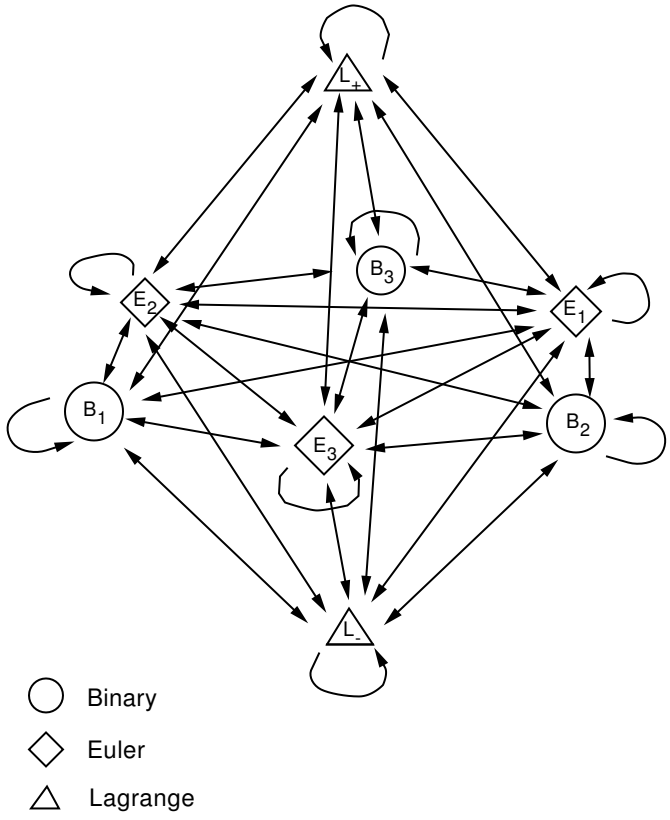

FIGURE 2. Graph of Boxes and Poincaré Mappings

The construction of the boxes and Poincaré mapping depend on several lemmas whose proofs require some restriction on the masses and on the angular momentum. Specifically, the masses must be chosen so that certain eigenvalues are nonreal and certain manifolds are transverse. There are no smallness conditions on the masses however. In addition, the angular momentum must be small so that the Eulerian and Lagrangian orbits pass sufficiently close to triple collision. In fact, the proof is by perturbation from the zero angular momentum case. These restrictions will be introduced in due course.

The results of the paper can be summarized as follows:

Theorem 1. *Consider the planar three-body problem with fixed negative energy and angular momentum, with the translational and rotational symmetries eliminated and with the double collisions regularized. If the angular momentum is nonzero but sufficiently small and if the masses are chosen in a certain large open set, then every path in figure 2 is realized by at least one solution. Moreover, every periodic path is realized by at least one periodic solution.*

1.2. **Some History.** To place the present paper in context it is necessary to recall some of the previous contributions. As was already mentioned above, the central

configurations were discovered in the eighteenth century by Euler and Lagrange [10, 13].

The study of triple collision was begun by Sundman [33] and continued by Siegel [30, 29]. McGehee introduced coordinates, described in section 2 below, which replaced the triple collision singularity by an invariant boundary manifold. All triple collision solutions converge to this boundary manifold. He used these coordinates in a qualitative study of the collinear three-body problem [16, 17]. Several authors applied these coordinates to the study of another special case: the planar isosceles three-body problem [5, 6, 11, 12, 18, 31]. In particular [6, 18] introduce symbolic dynamics into this problem in the zero angular momentum case. The author studied near-collision orbits in the planar three-body problem [22]. The symbolic dynamics introduced there corresponds to the part of figure 2 which does not involve the vertices B_j.

Oscillation, capture and escape orbits were studied by Sitnikov and Alexeev in a special case of the three-dimensional three-body problem, now called the Sitnikov problem [32, 1, 2, 3]. This is the subsystem which arises when one mass is moves along an axis while two equal masses move symmetrically around the axis. Sitnikov studied the restricted version of this where the body on the axis has zero mass and proved the existence of oscillation, capture and escape orbits. A geometrical account of this using symbolic dynamics is contained in [24]. This approach uses another coordinate system of McGehee (see section 2) to paste a two-dimensional boundary manifold at infinity to the three-dimensional constant energy manifold. All parabolic and hyperbolic orbits tend to this boundary manifold. In particular, there is a single periodic orbit at infinity to which all parabolic orbits converge. McGehee showed that the parabolic solutions form the analytic stable and unstable manifolds of this periodic orbit [15]. The introduction of symbolic dynamics is possible because of the existence of transversal intersections of these manifolds, that is, because there is a transversal homoclinic orbit to parabolic infinity. A similar approach has been used in other subsystems of two degrees of freedom such as the collinear problem and the restricted planar problem [14, 34].

Attempts to generalize this approach to the planar problem are hampered by the extra degree of freedom. The geometrical study of the behavior near infinity in the planar problem was begun by Easton and McGehee [9]. The boundary manifold at infinity is now four-dimensional. The parablic orbits of the planar three-body problem are the stable and unstable manifolds of an invariant three-dimensional sphere within this boundary manifold. The reason it is an invariant three-sphere instead of a periodic orbit as in the Sitnikov problem is that it represents all possible limiting motions of the binary as the distance to the third mass approaches infinity. This set of limiting motions is just the set of all two-body motions with fixed energy; after Levi-Civita regularization, this is just a three-sphere. The stable and unstable manifolds of the three-sphere are each four-dimensional. Easton showed that these manifolds are Lipschitz [7]. Robinson showed that they are analytic away from the three-sphere at infinity and C^∞ even at the three-sphere. He went on to show that orbits in these invariant manifolds converge to a single two-body orbit within the three-sphere [26, 27]. In [9] and [26] it is shown that symbolic dynamics could be introduced into the planar problem provided an appropriate homoclinic orbit to the invariant three-sphere could be found. The homoclinic orbit would

have to satisfy three conditions. First, it must be asymptotic to the same two-body orbit within the three-sphere in both forward and backward time. Second, it should represent a transverse intersection of the stable and unstable manifolds of the three-sphere. A third condition is required because of the degeneracy of the flow within the invariant three-sphere. As is well-known, the two-body flow with fixed negative energy consists entirely of periodic orbits of the same period. Thus a Poincaré mapping of a two-dimensional section along any given orbit is the identity mapping. The third requirement on the homoclinic orbit is that these two neutral directions should be hyperbolically stretched during the part of the homoclinic motion far from infinity. Unfortunately, it has never been possible to rigorously verify this third hypothesis although some progress has been made on numerical verification [8, 25]. (But see [35] for a different approach to proving existence of oscillation orbits.)

In [20] the author considered the Sitnikov problem with small angular momentum. A combination of the techniques used for the zero angular momentum case (which is just the planar isosceles problem) and those used to study the periodic orbit near infinity made it possible to introduce a symbolic dynamical description of an invariant set containing both close approaches to collision and excursions near infinity. The present paper uses the same approach for the planar problem. Although this approach does not directly involve construction of a homoclinic orbit to parabolic infinity, the existence of such orbits follows from theorem 1. The difficulty regarding the two neutral directions at infinity is overcome by the hyperbolic stretching produced near triple collision.

As mentioned already, the parts of figure 2 and theorem 1 which refer only to refer exclusively to near-collision orbits were already proved in [22]. Thus the main goal the present paper is to show how to incorporate excursions near infinity into the picture.

2. Coordinates and Equations of Motion

In this section, the equations of motion for the planar three-body problem will be written in several coordinate systems. In addition, the constants of motion will be given and the collinear invariant manifold introduced.

2.1. **Cartesian Coordinates.** The three-body problem concerns the motion of three point masses, m_1, m_2, m_3, moving under the influence of their mutual gravitational attraction. In this paper the particles are restricted to a plane. Let $q_j \in \mathbf{R}^2$ be their positions and $p_j = m_j \dot{q}_j \in \mathbf{R}^2$ be their momenta and set $q = (q_1, q_2, q_3) \in \mathbf{R}^6$ and $p = (p_1, p_2, p_3) \in \mathbf{R}^6$. Then the motion is described by the Hamiltonian system with Hamiltonian:

$$H(q,p) = \frac{1}{2}\, p^T A^{-1} p - U(q)$$

where q and p are thought of as column vectors, the superscript T denotes the transpose, A denotes the 6×6 mass matrix $\operatorname{diag}(m_1, m_1, m_2, m_2, m_3, m_3)$ and $U(q)$ is the Newtonian potential function:

$$U(q) = \frac{m_1 m_2}{|q_1 - q_2|} + \frac{m_1 m_3}{|q_1 - q_3|} + \frac{m_2 m_3}{|q_2 - q_3|}.$$

Hamilton's equations are:

$$\dot{q} = A^{-1}p$$
$$\dot{p} = U_q.$$

This gives a dynamical system on the space $\mathbf{R}^6\backslash\Delta \times \mathbf{R}^6$ where $\Delta = \{q : q_i = q_j \text{ for some } i \neq j\}$.

Using the familiar constants of motion, the problem can be reduced to a flow in five dimensions. First fix the total momentum to be zero, without loss of generality:

$$p_1 + p_2 + p_3 = 0.$$

Then the center of mass is constant and may be taken as zero:

$$m_1q_1 + m_2q_2 + m_3q_3 = 0.$$

Next one can fix the angular momentum:

$$p_1 \times q_1 + p_2 \times q_2 + p_3 \times q_3 = \omega$$

and the energy:

$$H(q,p) = h < 0.$$

These equations determine a six dimensional subset of $\mathbf{R}^6\backslash\Delta \times \mathbf{R}^6$ which will be denoted $\tilde{M}(h,\omega)$. Finally, there is a rotational symmetry. If one ignores an angular variable corresponding to rotation of all positions and momenta, one obtains a five-dimensional system. To put it another way, one can pass to a dynamical system on a five-dimensional quotient manifold, $M(h,\omega)$.

2.2. **Coordinates Near Triple Collision.** To study motion near triple collision, it is convenient to introduce new variables due to McGehee [17]. First let

$$r = \sqrt{q^T A q}$$

denote the square root of the moment of inertia. Because the center of mass is at the origin, this quantity measures the size of the triangle formed by the three bodies. In particular, $r = 0$ represents triple collision. Next introduce rescaled position and momentum variables:

$$s = \frac{q}{r}$$
$$z = \sqrt{r}p.$$

With the timescale $' = r^{\frac{3}{2}}\cdot$, the equations become:

$$r' = vr$$
$$s' = A^{-1}z - vs$$
$$z' = U_s(s) + \frac{1}{2}vz$$

where $v = s^T z$. The homogeneity of U is used to replace $U(q)$ by $U(s)$. The equations which define $\tilde{M}(h,\omega)$ become:

$$\begin{aligned} z_1 + z_2 + z_3 &= 0 \\ m_1s_1 + m_2s_2 + m_3s_3 &= 0 \\ s^T As &= 1 \\ \frac{1}{2}z^T A^{-1}z - U(s) &= hr \end{aligned} \tag{1}$$

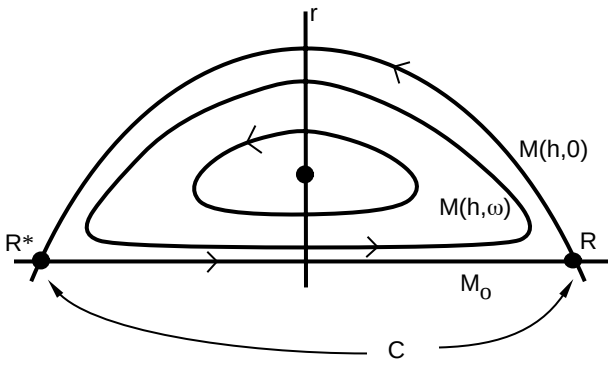

FIGURE 3. Collision Manifolds and a Restpoint Cycle

and

$$\sqrt{r}\,[z_1 \times s_1 + z_2 \times s_2 + z_3 \times s_3] = \omega. \tag{2}$$

These equations extend the vectorfield to $\{r = 0\}$. There are two subsets of $\{r = 0\}$ which are relevant to the study of near-collision orbits. By a theorem of Sundman [33], triple collisions can occur only for $\omega = 0$. Consider what happens to equation (2) above in this case. Let Ω denote $z_1 \times s_1 + z_2 \times s_2 + z_3 \times s_3$. Then the manifold $\tilde{M}(h, 0)$ is given by:

$$\tilde{M}(h, 0) = \{(r, s, z) : r > 0,\ (1) \text{ hold}, \Omega = 0\}.$$

Thus the set

$$\tilde{C} = \{(0, s, z) :\ (1) \text{ hold}, \Omega = 0\}$$

is sort of boundary manifold for $\tilde{M}(h, 0)$ at triple collision. This is the so-called collision manifold. There is a quotiented version of the collision manifold, denoted C, which is a four-dimensional boundary for the five-dimensional manifold $M(h, 0)$. The flow in the manifold C reflects the behavior of near-collision orbits with zero angular momentum.

Note, however that (1) can be solved without setting $\Omega = 0$. Let

$$\tilde{M}_0 = \{(0, s, z) :\ (1) \text{ hold},\ \ \Omega \geq 0\}.$$

Then the quotiented version, M_0, is a five-dimensional subset of $\{r = 0\}$ which is relevant to the study of the behavior of near-collision orbits with positive angular momentum. M_0 is a manifold with boundary; the boundary is just C. The relationship of the manifolds $M(h, \omega)$, $M(h, 0)$, M_0, and C is shown schematically in figure 3. This figure is really a picture of a sequence of periodic orbits in $M(h, \omega)$ converging to a cycle of restpoints in $M(h, 0) \cup M_0$ as $\omega \to 0$. This will be explained in section 3.

2.3. **Coordinates Near Infinity.** When the separation of the binary and the third mass is large, one expects the influence of the third mass on the binary to become negligible. Thus the flow near infinity in $M(h, \omega)$ can be understood intuitively as a product of the Keplerian motion the binary and the motion of the third mass relative to the center of mass of the binary. In this section, coordinates

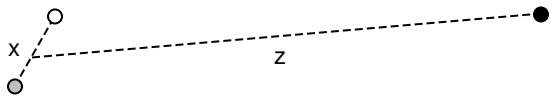

FIGURE 4. Jacobi Variables

are introduced which reflect this splitting. In what follows, m_3 is the "third mass" and the constants $\mu = m_1 + m_2$ and $M = m_1 + m_2 + m_3$ will be used frequently.

It is appropriate to introduce Jacobi variables as shown in figure 4. More precisely, let

$$x = q_2 - q_1$$
$$z = q_3 - \mu_1 q_1 - \mu_2 q_2$$

where $\mu_j = \frac{m_j}{\mu}$. Let $\xi = \dot{x}$ and $\zeta = \dot{z}$. Then the differential equations are:

$$\begin{aligned} \dot{x} &= \xi \\ \dot{\xi} &= \alpha^{-1} U_x \\ \dot{z} &= \zeta \\ \dot{\zeta} &= \beta^{-1} U_z \end{aligned} \tag{3}$$

where $\alpha = \frac{m_1 m_2}{\mu}$, $\beta = \frac{m_3 \mu}{M}$, and

$$U(x,z) = \frac{m_1 m_2}{|x|} + \frac{m_2 m_3}{|z - \mu_1 x|} + \frac{m_1 m_3}{|z + \mu_2 x|}.$$

The energy equation in these coordinates is:

$$H = \frac{1}{2}\left(\alpha|\xi|^2 + \beta|\zeta|^2\right) - U(x,z) = h.$$

Next we introduce coordinates (again due to McGehee [15]) which extend the flow to a boundary manifold at infinity. Let

$$z = \rho^{-2} e^{i\theta} \qquad \rho = \frac{1}{\sqrt{|z|}}$$

and decompose ζ into radial and angular parts:

$$\zeta = \nu \left(\frac{z}{|z|}\right) + \hat{\omega} \left(\frac{z}{|z|}\right)_{\perp}.$$

Then in the quotient manifold $M(h,\omega)$ one can ignore θ and eliminate $\hat{\omega}$ using the angular momentum integral. The resulting equations are:

$$\begin{aligned} \dot{\rho} &= -\frac{1}{2}\nu\rho^3 \\ \dot{\nu} &= -M\rho^4 + O(\rho^6) \end{aligned} \tag{4}$$

describing the motion of the third mass m_3 with respect to the binary, and:

$$\begin{aligned} \dot{x} &= \xi \\ \dot{\xi} &= -\frac{\mu x}{|x|^3} + O(\rho^4) \end{aligned}$$

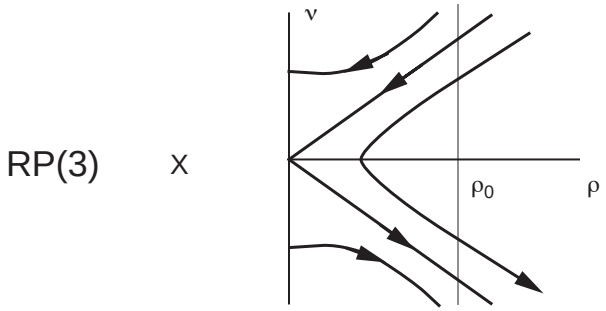

FIGURE 5. A Neighborhood of Infinity

describing the motion of the binary.

To lowest order in ρ the flow is a product of a simple flow in the (ρ, ν)-plane and the flow of the two-body problem (see figure 5). The four-dimensional invariant manifold $\{\rho = 0\}$ corresponds to $|z| = \infty$. Here the motion of (x, ξ) is described exactly by the two-body problem. More precisely, fixing the value $\nu = \nu_0$ corresponds to fixing the limiting velocity of separation of the third mass from the binary at infinity and the corresponding motions of (x, ξ) give a two-body problem with negative energy. Now the two-body problem with fixed negative energy and regularized double collisions is equivalent to the geodesic flow on the the unit tangent bundle of the round two-dimensional sphere [23]. This bundle is just an $RP(3)$. Alternatively, if Levi-Civita regularization is used, it is equivalent to the Hopf flow on S^3 [9]. Thus a neighborhood of infinity in $M(h, \omega)$ is diffeomorphic to a subset of the form $0 \leq \rho \leq \rho_0$ in the (ρ, ν) half-plane crossed with $RP(3)$. It is important to understand which properties of the product flow of figure 5 remain valid in such a neighborhood when the higher order terms in ρ are taken into account. Results of Easton, McGehee and Robinson show that the most important properties are preserved. These results will be discussed in section 4.

2.4. **The Collinear Submanifold.** The collinear three-body problem concerns the motion of three point masses on a fixed line. This can be viewed as a subsystem of the zero angular momentum planar problem. In fact, up to rotation, there are three such subsystems, $\mathcal{C}_j$, where the subscript indicates which mass lies between the other two on the line. These three-dimensional subsystems were studied by McGehee [16]. They will play an important role in this paper. In this section, the coordinates introduced above will be specialized to the collinear case. Let the positions of the particles be $q_j \in \mathbf{R}^1$, $j = 1, \ldots, 3$ where $q_1 < q_2 < q_3$.

2.4.1. *Near Collinear Infinity.* For the study of orbits which tend to infinity with m_1 and m_2 forming a binary system, it is convenient to introduce Jacobi variables as above. The differential equations are equations (3) where now x, ξ, z, and ζ are scalars.

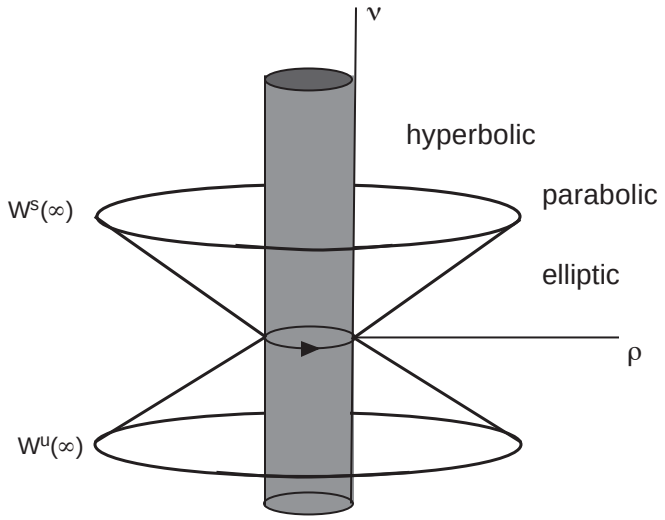

FIGURE 6. A Neighborhood of Collinear Infinity

McGehee's variables near infinity are $\rho = \frac{1}{\sqrt{z}}$ and $\nu = \zeta$. The collinear analogue of equations (4) are:

$$\begin{aligned} \dot{\rho} &= -\frac{1}{2}\nu\rho^3 \\ \dot{\nu} &= -M\rho^4\left[\frac{\mu_2}{(1-\mu_1 x\rho^2)^2} + \frac{\mu_1}{(1+\mu_2 x\rho^2)^2}\right]. \end{aligned} \tag{5}$$

The equations for x and ξ are approximately those of the collinear two-body problem with negative energy. The collinear two-body problem is very simple; after regularizing double collisions, the relative motion of masses m_1 and m_2 is a periodic bounded oscillation with repeated bounces. Thus in place of the $RP(3)$ in figure 5 there is a single periodic orbit. Ignoring the higher order terms as before, the flow in the three-dimensional energy manifold will be as in figure 6.

2.4.2. *Near Collinear Collision.* Near triple collision, introduce the variables (r, v, θ, w):

$$\begin{aligned} r^2 &= \alpha x^2 + \beta z^2 \\ \sqrt{r}v &= \alpha x\xi + \beta z\zeta \\ \tan\theta &= \sqrt{\frac{\beta}{\alpha}}\frac{z}{x} \\ \sqrt{r}w &= \sqrt{\alpha\beta}(x\zeta - z\xi). \end{aligned}$$

The variable r is again the square root of the moment of inertia while θ describes the relative spacing of the masses along the line. The value $\theta_{23} = \arctan(\sqrt{\frac{m_1 m_3}{M m_2}})$ represents a double collision of m_2 and m_3 while $\theta_{12} = \frac{\pi}{2}$ represents a double collision of m_1 and m_2. The meaning of v and w is apparent from the differential

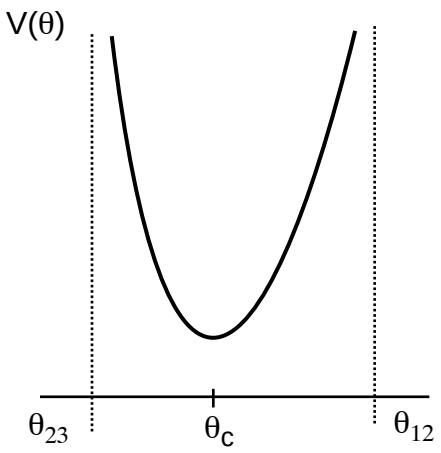

FIGURE 7. Potential of the Collinear Problem

equations below. After rescaling by a factor of $r^{\frac{3}{2}}$, the differential equations become:

$$\begin{aligned} r' &= vr \\ v' &= \frac{1}{2}w^2 + hr \\ \theta' &= w \\ w' &= V'(\theta) - \frac{1}{2}vw \end{aligned} \tag{6}$$

where

$$V(\theta) = \frac{m_1 m_2 \sqrt{\alpha}}{\cos\theta} + \frac{m_1 m_3 \sqrt{\alpha\beta}}{\sqrt{\alpha}\sin\theta + \mu_2\sqrt{\beta}\cos\theta} + \frac{m_2 m_3 \sqrt{\alpha\beta}}{\sqrt{\alpha}\sin\theta - \mu_1\sqrt{\beta}\cos\theta}.$$

The energy equation becomes:

$$\frac{1}{2}\left(v^2 + w^2\right) - V(\theta) = hr.$$

The behavior of $V(\theta)$ is shown in figure 7. It is singular at the double collisions and convex in between with a unique critical point $\theta = \theta_c(m_1, m_2, m_3)$. This θ-value corresponds to Euler's unique collinear central configuration for these masses [10].

Equations (6) still have double collision singularities but these can be eliminated by further analytic coordinate changes. Namely, if w is replaced by $\hat{w} = wf(\theta)$ where $f(\theta) = \cos\theta(\sqrt{\alpha}\sin\theta - \mu_1\sqrt{\beta}\cos\theta)$ and if the vectorfield is scaled by a factor of $f(\theta)$ then (6) becomes:

$$\begin{aligned} r' &= f(\theta)vr \\ v' &= f(\theta)V(\theta) + 2hf(\theta)r - \frac{1}{2}f(\theta)v^2 \\ \theta' &= \hat{w} \\ \hat{w}' &= f(\theta)^2 V'(\theta) - \frac{1}{2}f(\theta)v\hat{w} + f'(\theta)\hat{w} \end{aligned} \tag{7}$$

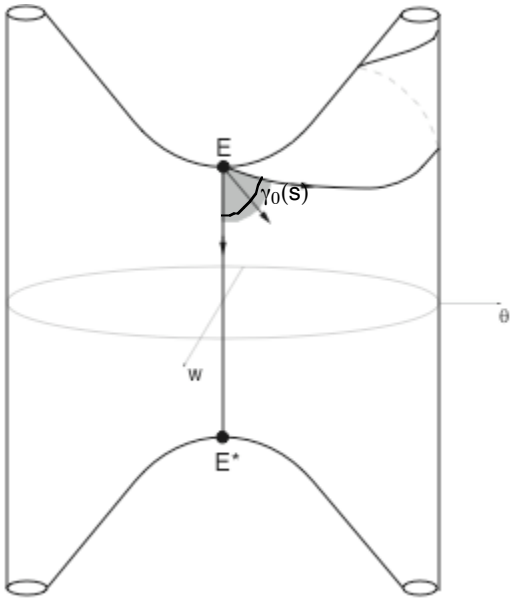

FIGURE 8. The Collinear Three-Body Problem

and the energy equation becomes:

$$K(\theta, v, \hat{w}) = \frac{1}{2}\left(f(\theta)^2 v^2 + \hat{w}^2\right) - f(\theta)^2 V(\theta) = h f(\theta)^2 r. \tag{8}$$

The functions $f(\theta)V(\theta)$ and $f(\theta)^2 V'(\theta)$ are analytic even at the double collisions. In these variables, the three-dimensional energy manifold can be visualized as the inside of the surface $K(\theta, v, \hat{w}) = 0$ in $(\theta, v, \hat{w})$-space (see figure 8). This surface is just the collinear triple collision manifold. The figure also shows Euler's homothetic orbit as a restpoint connection and several other features which will be explained later.

2.4.3. *A Limiting Case.* The results about the collinear problem needed below will be proved first for a special case where the central mass, m_2, is much larger than the other two masses, which are assumed equal. Set $m_1 = m_3 = 1$ and $m_2 = \frac{1}{\epsilon}$ where $\epsilon > 0$. Then $\alpha = \frac{1}{1+\epsilon}$ and $\beta = \frac{1+\epsilon}{1+2\epsilon}$.

Introduce a new timescale $' = \sqrt{\epsilon}\,\cdot$ and let $\xi = x'$ and $\zeta = z'$ now stand for the velocities with respect to the new time parameter. Then equations (3) become:

$$\begin{aligned} x' &= \xi \\ \xi' &= \alpha^{-1}\bar{U}_x \\ z' &= \zeta \\ \zeta' &= \beta^{-1}\bar{U}_z \end{aligned} \tag{9}$$

where

$$\bar{U} = \epsilon U = \frac{1}{x} + \frac{1}{z - \frac{\epsilon}{1+\epsilon}x} + \frac{\epsilon}{z + \frac{1}{1+\epsilon}x}.$$

The energy relation is:

$$\frac{1}{2}\left(\alpha\xi^2 + \beta\zeta^2\right) - \bar{U}(x,z) = \bar{h}$$

where $\bar{h} = \epsilon h$. In the limit $\epsilon \to 0$, (9) show that x and z are solutions of two-body problems which are coupled only by the requirement that the sum of their energies be $\bar{h}$.

Equations (5) describing the behavior at infinity are now:

$$\rho' = -\frac{1}{2}\nu\rho^3$$
$$\nu' = -\frac{1+2\epsilon}{1+\epsilon}\rho^4\left[\frac{1}{(1-\frac{\epsilon}{1+\epsilon}x\rho^2)^2} + \frac{\epsilon}{(1+\frac{1}{1+\epsilon}x\rho^2)^2}\right]$$

where ν is the new ζ.

The equations (7) describing the behavior near triple collision are changed only in that the velocities, v, w are rescaled by $\sqrt{\epsilon}$ and that $V(\theta)$ is replaced by:

$$\bar{V}(\theta) = \epsilon V(\theta) = \frac{\sqrt{\alpha}}{\cos\theta} + \frac{\sqrt{\alpha\beta}}{\sqrt{\alpha}\sin\theta - \frac{\epsilon}{1+\epsilon}\sqrt{\beta}\cos\theta} + \frac{\epsilon\sqrt{\alpha\beta}}{\sqrt{\alpha}\sin\theta + \frac{1}{1+\epsilon}\sqrt{\beta}\cos\theta}.$$

The energy equation becomes:

$$K(\theta, v, \hat{w}) = \frac{1}{2}\left(f(\theta)^2 v^2 + \hat{w}^2\right) - f(\theta)^2\bar{V}(\theta) = \bar{h}f(\theta)^2 r.$$

All of these equations depend analytically on ϵ even at $\epsilon = 0$.

3. Behavior Near Triple Collision

In this section some of the possible behaviors of near-collision orbits of the three-body will be described. Most of the results were proved in [22] but it is necessary to recall them before proceeding to the study of excursions near infinity. Some restrictive assumptions on the masses needed in [22] will be eliminated here.

Figure 3 was introduced as a schematic picture of the triple collision manifolds but it is really a picture of another important feature of the three-body problem: periodic orbits and restpoint cycles arising from the central configurations of Euler and Lagrange. Up to rotation and scaling, there are just five central configurations. The collinear or Eulerian configurations will be denoted e_j if the ordering is the one with m_j in the middle. The equilateral or Lagrangian ones will be denoted l_+ and l_- according to whether the masses m_1, m_2, m_3 occur in counterclockwise or in clockwise order around the triangle.

Lagrange demonstrated that each central configuration gives rise to a family of periodic solutions with nonzero angular momentum. For fixed values of $h < 0$ and ω (not too large) there will be exactly five such periodic orbits in $M(h,\omega)$, one for each central configuration (see figure 1). In the limit as $\omega \to 0$, the eccentricity of these elliptical orbits approaches 1 and one obtains homothetically expanding and contracting triple collision orbits.

With the changes of variables and of timescale of section 2.2, triple collision solutions converge to restpoints in the triple collision manifold, C. There are exactly 10 restpoints in C, two for each of the five central configurations: $r = 0$, $s = s_c$, $z = vAs_c$, $v = \pm\sqrt{2U(s_c)}$, where $s_c \in \{l_+, l_-, e_1, e_2, e_3\}$. The restpoints corresponding to $s_c = l_+$ will be denoted L_+, L_+^* where the star stands for the choice of the

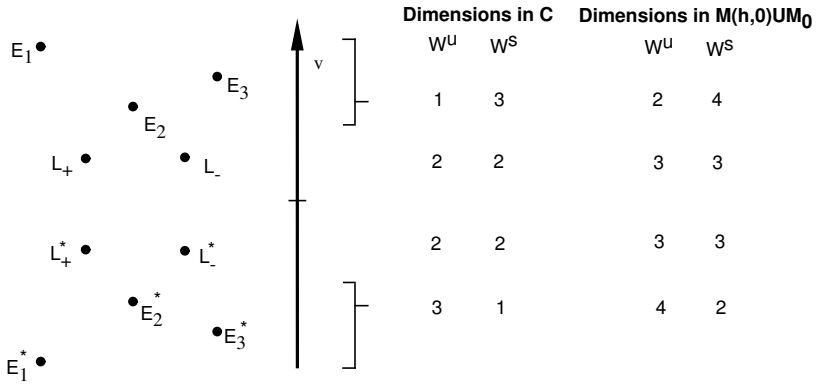

FIGURE 9. The Restpoints

minus sign for v; the other restpoints will be named in a similar way. These ten restpoints are the endpoints of the five homothetic triple collision orbits of Euler and Lagrange. Figure 3 shows such an orbit as a restpoint connection $R \to R^*$ in $M(h,0)$, where $R \in \{L_+, L_-, E_1, E_2, E_3\}$. There is also a connection $R^* \to R$ in M_0 shown in the figure. This represents the spinning behavior of the elliptical periodic solutions of nonzero angular momentum near triple collision. Intuitively, a highly eccentric elliptical orbit as in figure 1 can be viewed as a nearly homothetic expansion away from collision and contraction back toward collision followed by a very quick rotation by 360° near collision. In the limit as $\omega \to 0$, these periodic orbits converge to a restpoint cycle as in figure 3 with the restpoint connection in $M(h,0)$ representing the homothetic expansion and contraction and the connection in M_0 representing the spinning.

The restpoints are especially important in light of the fact that the flow in C (and indeed even in M_0) is gradient-like. The function $v = s^T z$ is strictly increasing along all non-stationary orbits. There are many triple collision orbits besides the five homothetic ones. However, they all converge to the set of restpoints in C. The restpoints are all hyperbolic and so have analytic stable and unstable manifolds. Orbits which tend to triple collision in forward time make up the five stable manifolds $W^s(R^*)$ while orbits tending to triple collision in backward time make up the five unstable manifolds $W^u(R)$. The dimensions of these stable and unstable manifolds are given in figure 9; the restpoints are shown arranged by v-value, then the first column give the dimensions as viewed in the four-dimensional collision manifold, C and the second gives the dimensions as viewed in the five-dimensional manifold-with-corners, $M(h,0) \cup M_0$. A glance at figure 3 will explain the fact that both the stable and unstable manifolds gain one dimension in the latter space.

Consider the question of transversality of the restpoint connection which make up the Eulerian and Lagrangian restpoint cycles. Figure 9 shows that in the Lagrangian case, all stable and unstable manifolds have dimension three in the five-dimensional set $M(h,0) \cup M_0$. Thus it is possible for both of the restpoint connections to be transverse intersections of the corresponding stable and unstable manifolds. For

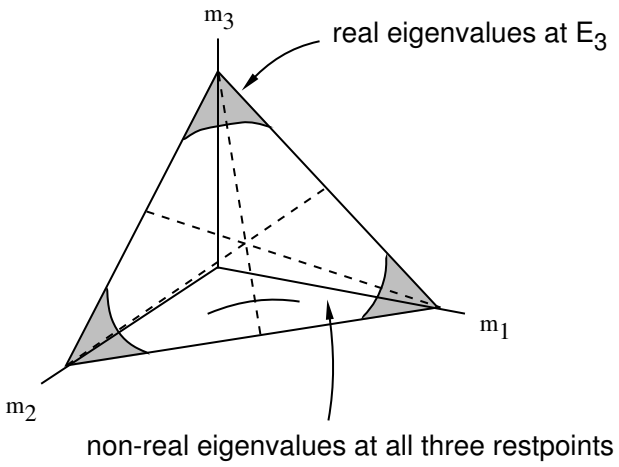

FIGURE 10. The Mass Triangle ($m_1 + m_2 + m_3 = 1$)

the connections $L_\pm \to L_\pm^*$ in $M(h,0)$ this was proved by Simo and Llibre and for the connections $L_\pm^* \to L_\pm$ in M_0 it was proved by the author for almost all choices of the masses.

Proposition 1. *For almost all masses, both of the Lagrangian restpoint connections are transverse.*

The Eulerian case seems puzzling. In particular, given the dimensions of $W^u(E_j)$ and $W^s(E_j^*)$, it is not clear why the connections $E_j \to E_j^*$ in $M(h,0)$ should exist. The explanation is that both $W^u(E_j)$ and $W^s(E_j^*)$ lie in the invariant three-dimensional collinear subsystem, $\mathcal{C}_j$. The two-dimensional manifolds $W^u(E_j)$ and $W^s(E_j^*)$ are entirely contained in $\mathcal{C}_j$. Devaney showed that the Eulerian homothetic solution (the vertical orbit in figure 8) is a transverse intersection of these stable and unstable manifolds when viewed in $\mathcal{C}_j$ [4].

Recalling that $\mathcal{C}_j$ is of codimension two in $M(h,0)$, it is natural to ask about the local behavior near E_j, E_j^* in the two dimensions complemetary to $\mathcal{C}_j$. It turns out that for most choices of the masses, the eigenvalues of E_j, E_j^* in these two directions are complex. They have negative real part at E_j and positive real part at E_j^*. Thus the flow near E_j, E_j^* tends to spiral around the codimension-two manifold, $\mathcal{C}_j$. This spiralling also plays a crucial role in what follows. The normalized masses for which this spiralling occurs are indicated in figure 10 which is based on [28].

Also important are the connections between the restpoints in C. For the purposes of this paper, only connections among the starred restpoints and among the unstarred ones are of interest. Because of the gradient-like property and the fact that the manifolds $W^u(E_j)$ and $W^s(E_j^*)$ lie in the collinear submanifolds, $\mathcal{C}_j$, the only possible connections are those between the Lagrangian restpoints and the Eulerian ones. The following result shows that all of these occur.

Proposition 2. *For almost all masses, there is at least one transverse connection from each of $L_\pm$ to each E_j and from each E_j^* to each of $L_\pm^*$ in C.*

Actually it was shown in [19] that there is always at least one topologically transverse connection, and in [22] that the proposition is true when two of the masses are nearly equal. The equal mass case is easier because of the existence of yet another invariant submanifold of $M(h, 0)$. Namely, in this case there is an invariant set, $\mathcal{I}_j$, of orbits for which the configuration is always an isosceles triangle with m_j on the axis of symmetry. There is an isoceles collision manifold of dimension two and the three-dimensional isosceles submanifold can be visualized as its interior. After regularizing double collisions it looks like figure 11. The gradient-like property forces the existence of unique connections between the Lagrangian and Eulerian restpoints in $\mathcal{I}_j$. In [22] it was shown that these are transverse even when viewed in the four-dimensional manifold C. This was proved by a consideration of the variational equations along the connecting orbits. It turns out that Proposition 2 follows from this result by an analyticity argument which will now be presented.

Consider the question of connections from $L_\pm$ to E_j. In the four-dimensional collision manifold, C, choose a three-dimensional level set of the Lyapunov function v between the levels of $L_\pm$ and E_j. In this level set, $W^s(E_j)$ has dimension 2 while $W^u(L_\pm)$ is a curve. By the results of [19] $W^u(L_\pm)$ must intersect all three of the Eulerian stable manifolds so it is not contained entirely in $W^s(E_j)$. It follows from analyticity of the stable and unstable manifolds that there are at most finitely many connections from $L_\pm$ to E_j. It was already mentioned that in the case of two equal masses, there is a unique connection in the isosceles submanifold $\mathcal{I}_j$ and that this connection is transverse. By symmetry, the number of non-isosceles connections must be even; indeed, $\mathcal{I}_j$ is the fixed manifold of an obvious involution of C and this involution establishes a pairing of the non-isosceles connections. It follows that when two masses are equal there must be an odd number of *transverse* connections from $L_\pm$ to E_j. It will now be shown that this last property holds for almost all masses. In particular, there must be at least one transverse connection as claimed in Proposition 2.

Consider an analytic curve of masses, $m_j(s)$, $-1 < s < 1$, like the one in figure 10. More precisely, suppose two masses are equal when $s = 0$ and that the curve is symmetric in the line of equal masses. It will be shown that there are at most finitely many values of s for which the number of transverse connections from $L_\pm$ to E_j is even. This is more than sufficient to establish the proposition.

A local analysis of each non-transverse connection is needed. Suppose that for some parameter s_0, there is such a connection. Locally, $W^s(E_j)$ can be represented as the zero set of an analytic function depending analytically on s and $W^u(L_\pm)$ as a parametrized curve, with parameter t. So their intersection is given by the zeroes of a real analytic function, $\Phi(s, t)$. By the Weierstrass preparation theorem, there is some $\delta > 0$ and a monic (leading coefficient 1) polynomial $P^s(t)$ with coefficients which are real analytic functions of s such that for $s \in [s_0 - \delta, s_0 + \delta]$, the zero set of $\Phi(s, t)$ agrees with that of $P^s(t)$. Let k denote the quotient field of the ring of functions which are real analytic in some neighborhood of s_0. This field consists of all real Laurent series convergent in some punctured neighborhood of s_0. Then the Weierstrass polynomial, $P^s(t)$, is an element of the unique factorization domain

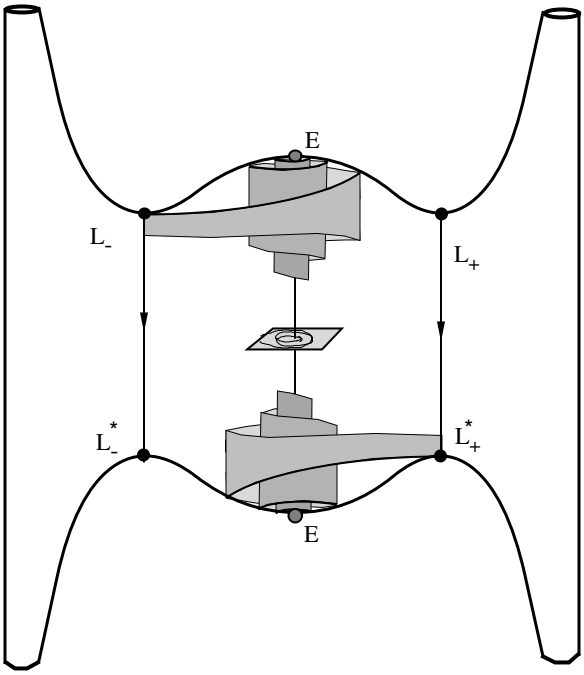

FIGURE 11. The Isosceles Three-Body Problem

$k[t]$ of polynomials over k. Therefore it can be factored as:

$$P^s(t) = \prod_{k=1}^{m} Q_k^s(t)^{\lambda_k}$$

where the $Q_k^s(t)$ are distinct, irreducible, monic polynomials in $k[t]$ and the λ_k are positive integers. The discriminant of an irreducible polynomial like $Q_k^s(t)$ is a nonzero element of k, that is, a nontrivial Laurent series in s. Moreover, since the leading coefficient never vanishes, the value of this discriminant at a fixed s_1 is the ordinary discriminant of the real polynomial $Q_k^{s_1}(t)$. It follows that the values of s for which $Q_k^s(t)$ has a repeated root are the zeroes of a nontrivial Laurent series and so do not accumulate at s_0. Similarly, the polynomials $Q_k^s(t)$ and $Q_l^s(t)$ for $l \neq k$ have a common root only when their resultant, also given by a nontrivial Laurant series in s, vanishes. Thus by taking δ smaller, if necessary, one may assume that all roots of the $Q_k^s(t)$ are distinct. It follows that for $s \in [s_0 - \delta, s_0 + \delta]$, $s \neq s_0$, the nondegenerate roots of $P^s(t)$ are precisely the roots of those $Q_k^s(t)$ for which $\lambda_k = 1$. Because the $Q_k^s(t)$ are real, the number of real, nondegenerate roots is constant in each of the intervals $(s_0, s_0 + \delta]$ and $[s_0 - \delta, s_0)$ and the difference of these two numbers is even.

Now it follows that along the one-parameter family there are finitely many values of s where the number of transverse connections changes and that if these are

deleted, the parity of the number of transverse connections is constant. It only remains to show that the parity is odd. For this, recall that at $s = 0$, the number of transverse connections is known to be odd. If $s = 0$ is not one of the finitely many bifurcation points, then the proof is complete. Even if it is one of the bifurcation points, it follows from the symmetry of the one-parameter family and the existence of the involution fixing the isosceles manifold that the number of new simple roots created as s moves away from 0 is even. For suppose that near a certain non-isosceles degenerate root, the number of non-degenerate roots changes from r to $r + 2k$ as s increases through 0. Then at the symmetrical non-isosceles root the change will be from $r + 2k$ to r and so the total number of non-degenerate roots arising from the symmetric pair of degenerate roots is $2r + 2k$ on both sides of $s = 0$. Thus for all s near 0 there are an odd number of transverse connections and hence this is true for all non-bifurcation points of the family.

Figure 11 shows the combined effect of the connections of Proposition 2 and the spiralling around the collinear restpoints. Part of $W^u(L_\pm)$ gets wrapped into a spiral converging down to $W^u(E_j)$. Similarly, a part of $W^s(L^*_\pm)$ spirals down to $W^s(E^*_j)$. Near the Eulerian homothetic orbit (which lies in both $W^u(E_j)$ and $W^s(E^*_j)$) there are infinitely many topologically transverse connections of the form: $L_\pm \to L^*_\pm$. Much of the papers [21] and [22] are devoted to extending these results to the planar problem. This extension is possible once the concept of a spiralling manifold is suitably defined.

The definition adopted here is designed to model the intuitive idea that a spiralling manifold should be a one-parameter family, S_θ, of copies of some core manifold, S_∞, parametrized by a polar coordinate θ. The polar angle, θ is defined in the complement of some codimension-two submanifold around which the spiralling takes place. The copies S_θ should converge in a controlled way to S_∞ as $\theta \to \infty$. The precise definition below is chosen to guarantee that the concept of spiral is independent of the choice of the polar coordinate system and is invariant under diffeomorphisms [21].

Definition 1. *Let Z be a compact manifold of dimension $n + 2$ and Y a compact submanifold of dimension n. Suppose that Y has a trivial tubular neighborhood so that polar coordinates can be introduced. Let S_∞ be a compact submanifold of Y. A submanifold $S \subset Z \backslash Y$ is a* **spiral around** Y **with core** S_∞ *if in some tubular neighborhood U of Y, S can be parametrized (in polar coordinates) as the image of a mapping $\sigma : S_\infty \times [\hat{\theta}, \infty) \to U \setminus Y \times D^2$ with the following properties:*

- *σ has the form $\sigma(u, \theta) = (y(u, \theta), \rho(u, \theta), \theta)$*
- *the embeddings $\sigma_\theta(u) = \sigma(u, \theta)$ converge in the C^1 topology to the inclusion $i : S_\infty \to Y$ as $\theta \to \infty$*
- *$\frac{\partial y}{\partial \theta}$ and $\frac{\partial \rho}{\partial \theta} \to 0$, as $\theta \to \infty$*

In [22] it is shown that on account of the transverse $L_\pm \to E_j$ connection and the spiralling at E_j, parts of $W^u(L_\pm)$ form spirals around the collinear manifold $\mathcal{C}_j$ with core $W^u(E_j)$. In spite of the high dimensions, it is possible to visualize this. Choose any point p in $W^u(E_j)$ and set up a four-dimensional cross-section to the flow at p. In this cross-section $\mathcal{C}_j$ will be a two-dimensional manifold. Introduce polar coordinates (ρ, θ) in the complementary two dimensions. Then the sets $\{\theta = \theta_0\}$ are three-dimensional half-spaces as in figure 12. The collinear manifold $\mathcal{C}_j$ appears as the two-dimensional plane $\rho = 0$ and within this plane, the unstable manifold

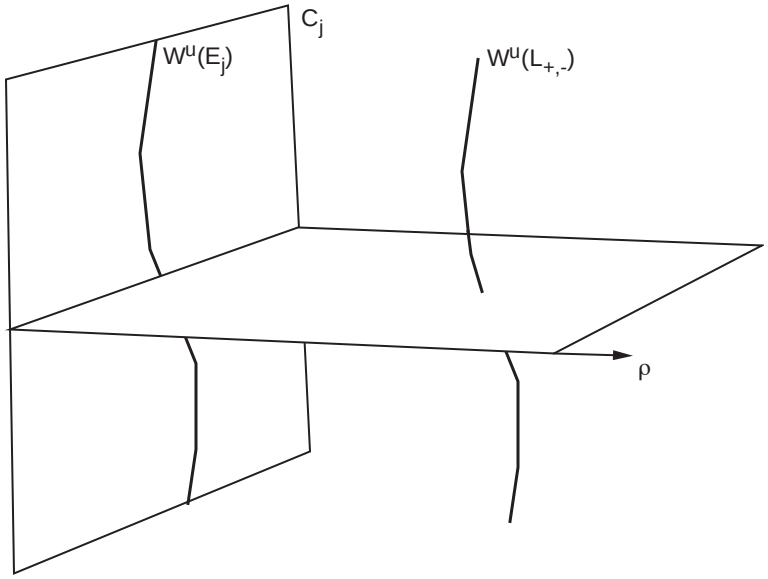

FIGURE 12. Spiralling of $W^u(L_\pm)$ around $W^u(E_j)$

$W^u(E_j)$ forms a curve. According to the definition of a spiral, parts of $W^u(L_\pm)$ near $\rho = 0$ will appear as curves which converge to the curve $W^u(E_j)$ as the parameter $\theta_0 \to \infty$. The horizontal plane in the figure will be explained later. The picture is the same near each $p \in W^u(E_j)$.

Similarly, parts of $W^s(L_\pm^*)$ spiral down to $W^s(E_j^*)$. In fact if p is chosen to be a point along Euler's homothetic orbit, both spirals will appear in the same picture. The curves representing $W^u(E_j)$ and $W^s(E_j^*)$ intersect transversely at p and the spirals move in opposite directions. The result is infinitely many intersections of $W^u(L_\pm)$ and $W^s(L_\pm^*)$ near p. Using analyticity one can show that these intersections are topologically transverse in the sense that there are C^0 local coordinates near the points of intersection making the surfaces $W^u(E_j)$ and $W^s(E_j^*)$ look like transverse coordinate planes in $\mathbf{R}^4$.

Proposition 3. *For all masses such that E_j and E_j^* have complex eigenvalues and such that there are transverse connections $L_\pm \to E_j$ and $E_j^* \to L_\pm^*$, there are infinitely many topologically transverse connections from each of $L_\pm$ to each of $L_\pm^*$. Moreover, these occur in every neighborhood of the Eulerian homothetic connection $E_j \to E_j^*$.*

According to Proposition 2, the masses such that the hypotheses are satisfied are almost all of the masses not in the shaded region associated to index j in figure 10. Thus, for almost all masses, the hypotheses will be satisfied for at least two values of j and for almost all masses in the large unshaded region of figure 10, all three values of j are allowed.

Figure 13 is a schematic picture of the many restpoint connections between Lagrangian restpoints in $M(h, 0)$. These were used in [22] as a framework for embedding symbolic dynamics. Each connection represents a topologically transverse intersection of stable and unstable manifolds. Thus in four-dimensional cross-sections

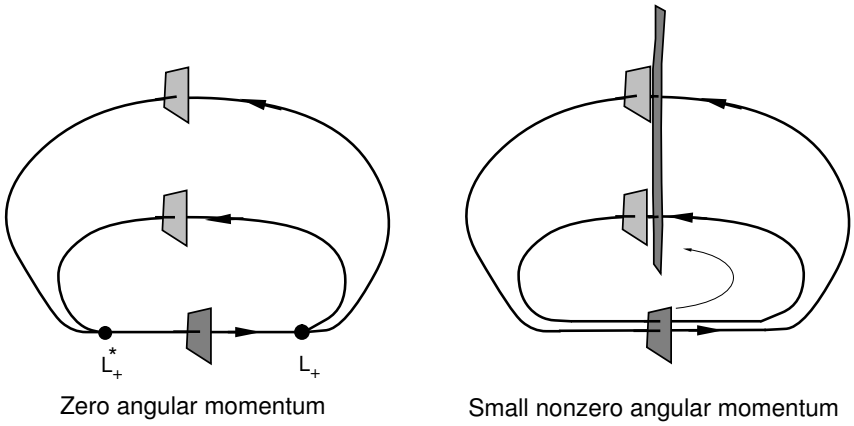

FIGURE 13. Poincaré Maps for Boxes near Collision

along each such orbit, C^0 coordinates can be found reducing the intersecting stable and unstable manifolds to coordinate planes. A four-dimensional cube in such a coordinate system will have two directions aligned with the stable manifold of a Lagrangian restpoint and the other two aligned with the intersecting unstable manifold. This implies that when such a cube is followed near the corresponding restpoints, it is stretched in a favorable way.

This network of stretching cubes gives rise to the symbolic dynamics when a small amount of angular momentum is supplied. This perturbation removes the restpoints and the flow near where the restpoints used to be carries the boxes which were aligned with the stable manifold across the neighborhood to the boxes which were aligned with the unstable manifold. Fixing attention to a finite number of boxes, one can prove that for sufficiently small but nonzero angular momenta, the flow in $M(h, \omega)$ stretches every incoming box across every outgoing box as in figure 13. The technical details of this perturbation were discussed in detail in [22] and will not be repeated here. However, since it will be necessary to construct more four-dimensional boxes to describe the dynamics near infinity, it is convenient to recall here which properties were necessary for the proof.

A four-dimensional box is a homeomorphic image of I^4 where $I = [-1, 1]$. Viewing I^4 as $I^2 \times I^2$ one can split the boundary ∂I^4 into two pieces, $\partial_+ = \partial I^2 \times I^2$ and $\partial_- = I^2 \times \partial I^2$. Each of these subsets is a solid torus and is therefore homologically a circle. The notation is meant to suggest that the first two dimensions are stretched and the last two contracted by the forward time flow. This "stretching" need not be of the type usually discussed for hyperbolic dynamical systems. Instead a weaker condition, based on singular homology theory is employed. Roughly speaking, the condition is that the circle generating the first homology of the ∂_+ of the first box is carried by the Poincaré map to a corresponding generator of the second box and similarly for the ∂_- and the inverse Poincaré map. The proofs in [22] show that if w_0 and w_1 are sufficiently small boxes transverse to the flow such that $\partial_+ w_0$ is linked with the stable manifold (which has codimension 2) of a Lagrangian restpoint while $\partial_- w_1$ is linked with the unstable manifold, then when a

sufficiently small amount of angular momentum is introduced w_0 is stretched across w_1 by the perturbed flow in the homological sense described above.

The results described in this section constitute the proof of the part of theorem 1 which refers to paths in figure 2 not involving excursions near infinity. In the sections that follow, the network will be extended to include boxes near infinity. According to the results cited in the last paragraph, it will be necessary to construct these boxes so that they are sufficiently small and are linked with the appropriate stable or unstable manifolds of Lagrangian restpoints.

4. Behavior Near Infinity

In this section, motions near infinity will be incorporated into the symbolic dynamical scheme of section 3.

4.1. **Flow Near Infinity.** In section 2.3 changes of variables were described which facilitate the qualitative study of the flow near infinity. As was mentioned there, the flow is approximately the product of the two-body flow, describing the behavior of the binary, and the flow of equations (4), describing the motion of the third mass relative to the center of mass of the binary. It is important to understand which properties of the product flow remain valid in such a neighborhood when the higher order coupling terms are taken into account.

From (4) it is clear that one can choose ρ_0 sufficiently small that estimates $-a\rho^4 < \dot{\nu} < -b\rho^4$ hold throughout $\{\rho < \rho_0\}$, where a and b are positive constants. It follows easily from this that any orbit in the neighborhood with $\nu(0) > 0$ falls into one of the following three classes:

- Hyperbolic: $\rho \to 0$, $\nu \to \nu_0 > 0$
- Parabolic: $\rho \to 0$, $\nu \to 0$
- Elliptic: ρ reaches a positive minimum and then increases to ρ_0.

A similar classification holds in backward time.

For the purposes of this paper, it is most important to understand the parabolic orbits, that is, the stable and unstable sets of the invariant $RP(3)$, $\{\rho = \nu = 0\}$. These will be denoted $W^{s,u}(\infty)$. As suggested by figure 5, these sets are locally four-dimensional manifolds. The difficulty in studying them is that on account of the factor of ρ^3 in equations (4), the invariant $RP(3)$ is not normally hyperbolic. Nevertheless, using ideas developed by McGehee in the two degree of freedom case, Easton was able to show that the parts of these stable and unstable sets with $\rho > 0$ are Lipschitz four-dimensional manifolds [7]. Robinson went on to show that they are real analytic and C^∞ even at $\rho = 0$ [26, 27]. Furthermore, he showed that each orbit in $W^{s,u}(\infty)$ converges to an individual orbit of the two-body problem. The orbit space of the two-body problem with fixed negative energy is a two-sphere; the points of the two-sphere represent possible ellipses with the semi-major axis fixed by the energy. Thus the fact that there is a well-defined limiting orbit means that there are maps $\omega^* : W^s(\infty) \to S^2$ and $\alpha^* : W^u(\infty) \to S^2$ assigning to each parabolic orbit its limiting binary behavior. Robinson showed that these maps are C^∞ and real analytic for $\rho > 0$.

Consider a Poincaré map near an orbit in the invariant $RP(3)$ at infinity. Unfortunately, the flow of the two-body problem on this $RP(3)$ does not have a global cross-section, although locally, of course, such cross-sections exist. Nevertheless, by abuse of illustration, several of the figures which follow are drawn as if there were

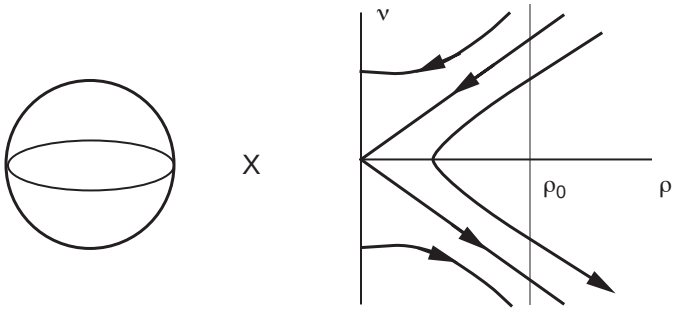

FIGURE 14. Poincaré Section Near Infinity

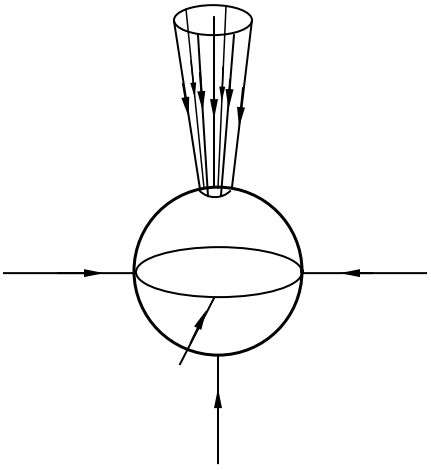

FIGURE 15. Inside the Stable Manifold of Infinity

an S^2 which was a global cross-section for the flow. This S^2 is naturally identified with the orbit space of the two-body problem since each two-body orbits hits the Poincaré section in a unique point. So a four-dimensional cross-section near infinity can be viewed as a part of S^2 crossed with the (ρ, ν) half-plane as in figure 14.

Because of the smoothness of the stable and unstable manifolds, one can introduce a new ν coordinate so that in the Poincaré section, $W^{s,u}(\infty)$ become products of the two-sphere with lines in the (ρ, ν) plane as in the figure. Locally, each of these manifolds is diffeomorphic to $S^2 \times [0, \rho_0)$ and because of Robinson's results about the smoothness of α^* and ω^* they are smoothly foliated into invariant curves over the two-sphere as in figure 15. It follows that there are C^∞ coordinates (ρ, ν, z) in the Poincaré section such that $z \in \mathbf{R}^2$ are local coordinates in the two-sphere and in $W^{s,u}(\infty)$ the foliations are given by setting z equal to a constant.

Recalling the differential equations 4, one finds that the Poincaré map in these coordinates takes the form:

$$\begin{aligned} \rho_1 &= \rho - \tfrac{1}{2}\nu\rho^3 + O(5) \\ \nu_1 &= \nu - M\rho^4 + O(5) \\ z_1 &= z + \rho^4 h(\rho, \nu, z) \end{aligned} \tag{10}$$

where $h(\rho, \nu, z)$ vanishes on $W^{s,u}(\infty)$. Here $O(5)$ means $O(|(\rho, \nu)|^5)$. Note that since $h(0, 0, z) = 0$, it follows that $z_1 = z + O(5)$.

4.2. **Connections Between Triple Collision and Infinity.** To incorporate excursions near infinity into the symbolic dynamics it is necessary to find orbits which connect a neighborhood of triple collision to a neighborhood of infinity. In this section, zero angular momentum solutions which have a triple collision in one time direction and tend parabolically to infinity in the other time direction will be constructed. In view of the results described in the last two sections, such solutions can be viewed as intersections of the stable and unstable manifolds of restpoints in the triple collision manifold, C, with the stable and unstable manifolds of the invariant $RP(3)$ at infinity.

4.2.1. *Connections in the Collinear Problem.* First consider one of the three collinear subsystems, $\mathcal{C}_j$. Recall from section 2.4 that these subsystems are three-dimensional. There is a single periodic orbit at parabolic infinity and it has analytic stable and unstable manifolds, $W^{s,u}(\infty)$, which divide a neighborhood of infinity into elliptic and hyperbolic regions (see figure 6). There is a two-dimensional triple collision manifold containing the restpoints E_j and E_j^*. These are saddle points when viewed in the triple collision manifold but $W^u(E_j)$ and $W^s(E_j^*)$ are two-dimensional in $\mathcal{C}_j$. They intersect transversely along Euler's orbit (see figure 8). Since the invariant manifolds of collision and infinity are both two-dimensional, it is possible to have isolated transverse connections between them.

Proposition 4. *For almost all masses, there is at least one transverse connecting orbit in $W^u(E_j) \cap W^s(\infty)$ and one in $W^s(E_j^*) \cap W^u(\infty)$ in the collinear subsystem $\mathcal{C}_j$.*

By time-reversal symmetry, it suffices to consider connections from collision to infinity.

The problem will be reduced to finding zeros of an analytic function along a curve. The first step is to represent a part of $W^s(\infty)$ as the zero-set of an analytic function. Let

$$\begin{aligned} \mathcal{U} &= \{(r, \theta, v, w) : H = h, r > 0, \theta_c \le \theta \le \pi/2, \sin\theta v + \cos\theta w \ge 0, w \ge 0\} \\ &= \{(x, \xi, z, \zeta) : H = h, z > 0, z \ge \kappa_c x, \zeta \ge 0, x\zeta - z\xi \ge 0\} \end{aligned}$$

where κ_c is the value of the ratio z/x at the Eulerian central configuration. $\mathcal{U}$ is the set where the shape of the collinear configuration is between the central configuration and the configurations with m_1, m_2 forming a tight binary, where the binary is becoming tighter, and where the seperation z between the binary and m_3 is increasing. This set includes a portion of the stable manifold $W^s(\infty)$.

In place of z, ζ or ρ, ν, introduce the functions $F = \rho\nu$, $G = \frac{1}{2}\nu^2 - M\rho^2$. On a manifold of fixed energy with double collisions between m_1, m_2 regularized, one can parametrize $\mathcal{U}$ by F, G, ψ where ψ is an angle representing the phase of the

binary motion. The part of $\mathcal{U}$ near infinity will be contained in the top half ($\nu \geq 0$) of figure 6 with F, G replacing ρ, ν. Now the differential equations (5) show that to lowest order, $W^s(\infty)$ is given by $G = 0$. McGehee's proof of analyticity of $W^s(\infty) \cap \{\rho > 0\}$ shows that this manifold can be expressed as a graph $G = \Psi(F, \psi)$ where Ψ is a real-analytic function, periodic in ψ. This representation will be valid for $0 < F < \delta$ for some $\delta > 0$. In particular, if one fixes a constant $c \in (0, \delta)$ then $W^s(\infty) \cap \{F = c\}$ is given by $\Phi(G, \psi) = G - \Psi(c, \psi) = 0$. Furthermore points with $\Phi > 0$ will be hyperbolic and those with $\Phi < 0$ will be elliptic.

The next step is to follow a part of $W^u(E)$ forward under the flow to the level set $\{F = c\}$. First note that for solutions in $\mathcal{U}$, (5) shows that the derivative of F along the flow satisifies:

$$\dot{F} = -\tfrac{1}{2}\nu^2\rho^3 - MB\rho^5 \leq -\tfrac{1}{2}\rho F^2 = -\tfrac{1}{2}\frac{F^3}{\nu}$$

where $B > 0$ is the quantity is square brackets in (5). This shows that F is decreasing along solutions. In $\mathcal{U}$ the quantities ρ and ν are also decreasing and it follows that for solution in $\mathcal{U} \cap \{F \geq c\}$ there is a negative upper bound

$$\dot{F} \leq -\tfrac{1}{2}\frac{c^3}{\nu_0}$$

where $\nu_0 > 0$ is the initial value of ν. Hence any solution with $F \geq c$ which remains in $\mathcal{U}$ eventually reaches the set $\{F = c\}$. On the other hand, solutions which leave $\mathcal{U}$ must do so by having $\zeta = 0$ which means $F = 0$. If initially $F \geq c$ then these solutions must also reach $\{F = c\}$.

Now consider the part of $W^u(E)$ with $\theta \geq \theta_c$ and $w \geq 0$. Note that at E one has $\sin\theta v + \cos\theta w \ = \sin\theta_c v_0 > 0$ so any sufficiently small part of $W^u(E)$ also satisfies $\sin\theta v + \cos\theta w \geq 0$ and so lies in $\mathcal{U}$ (see figure 8). Let $\gamma_0(s)$, $0 \leq s \leq 1$ be a small, analytic curve in $W^u(E) \setminus E$ such that $\gamma_0(0)$ lies on Euler's homothetic orbit and $\gamma_0(1)$ is in the collision manifold $\{r = 0\}$ (see figure 8). The values $F(\gamma_0(s))$ can be made arbirtrarily large by taking γ_0 sufficiently close to E since in McGehee coordinates, one has

$$F = \frac{\beta^{\frac{1}{4}}(\sin\theta v + \cos\theta w)}{r\sqrt{\sin\theta}}.$$

Note that $F \to \infty$ as $r \to 0$ so the point on the collision manifold, $\gamma_0(1)$, will be excluded below. If γ_0 is chosen so that $F(\gamma_0(s)) \geq c$, $0 \leq s < 1$ then one can follow these initial conditions forward under the flow to obtain a curve $\gamma(s)$ in $\{F = c\}$. Then finding transverse connections from E to infinity amounts to finding nondegenerate zeros of the analytic function Φ on $\gamma(s)$.

The quantities involved in this reduction can be made to depend analytically on the masses as well. For any choice of masses $m = (m_1, m_2, m_3)$, let γ_m denote the curve constructed above and Φ_m the analytic function. Recall that $\Phi_m = 0$ is part of $W^s(\infty)$, that is, the parabolic orbits. The elliptic orbits satisfy $\Phi_m < 0$ while the hyperbolic ones satisfy $\Phi_m > 0$. Now $\gamma_m(0)$ represents Euler's orbit, which is elliptic so $\Phi(\gamma_m(0)) < 0$. At the other end, $\gamma_m(1)$ is in the collision manifold. As shown in figure 8, this orbit spirals up one of the arms of the collision manifold. McGehee showed that nearby points not in the collision manifold tend to infinity hyperbolically with large limiting separation velocity. Thus $\Phi(\gamma_m(s)) > 0$ for s sufficiently close to 1. It follows that there exist zeroes of Φ along γ for all m. The problem is to show that at least one zero is nondegenerate.

This question will be resolved first in the special limiting case introduced in section 2.4.3. In this case, the middle mass, m_2, is much larger than the other two masses and the dynamics is just that of two separate collinear two-body problems, one with variables (x, ξ) describing the binary system composed of m_1 and m_2 and the other with variables (z, ζ) describing the motion of m_3 relative to m_2. The two problems are coupled only by the requirement that their total energy be fixed. The energy of the two-body problem for m_3 is $\frac{1}{2}\zeta^2 - \frac{1}{z} = G$. Clearly $z \to \infty$ parabolically if and only if this energy is zero. Therefore, in this limiting case, one knows the analytic function describing $W^s(\infty)$ explicitly: $\Phi(G, \psi) = G$. It will now be shown that there is a single point of intersection and that the intersection is transverse.

For this limiting case, the energy G is a constant of motion so it suffices to consider zeros of G on the initial curve $\gamma_0(s)$. It suffices to approximate $W^u(E)$ by its tangent plane near E. Using (r, v, θ, w) as coordinates, $E = (0, v_0, \pi/4, 0)$ where $v_0 = 2^{5/4}$. Calculating the eigenvectors at E shows that the two-dimensional tangent plane to $W^u(E)$ can be parametrized as

$$(\delta r, \delta v, \delta\theta, \delta w) = \delta v(-v_0, 1, 0, 0) + \delta w(0, 0, v_0, 1)$$

where the rescaled energy from section 2.4.3 has been taken as $\bar{h} = -1$ without loss of generality. One can choose

$$\gamma_0(s) \approx (0, v_0, \pi/4, 0) - \epsilon \cos s(-v_0, 1, 0, 0) + \epsilon \sin s(0, 0, v_0, 1)$$

where $\epsilon > 0$ is a small constant. Now

$$G = \tfrac{1}{2}\zeta^2 - \frac{1}{z} = \frac{1}{r}\left(\tfrac{1}{2}(\sin\theta v + \cos\theta w)^2 - \frac{1}{\sin\theta}\right)$$

and one finds

$$G(\gamma_0(s)) \approx \tfrac{1}{2}((1 + 6\sqrt{2})\tan s - 1).$$

It is easy to check that this function has exactly one zero for $0 \le s < 1$ and it is nondegenerate. The same will be true for the exact $\gamma_0(s)$ if ϵ is sufficiently small.

Next consider masses of the form $m = (1, \frac{1}{\epsilon}, 1)$ as in section 2.4.3. It was shown there that the differential equations depend analytically on ϵ, even at $\epsilon = 0$. It follows from the study of the limiting case above that for all sufficiently small ϵ, Φ will have a single zero along γ and it will be nondegenerate.

Finally consider any m. It can be connected by a line segment in mass space to one of these special masses. Let u, $0 \le u \le 1$, be a parameter along this line segment. Then for each u there is an analytic curve $\gamma_{m(u)}$, $0 \le s < 1$. and an analytic function $\Phi_{m(u)}$ as above. Define an analytic function of two variables by $\Phi(s, u) = \Phi_{m(u)}(\gamma_{m(u)}(s))$. Then the desired conclusion follows from an analyticity argument similar to that in section 3. Namely, the nondegenerate zeros of $\Phi(s, u_0)$ bifurcate in pairs as u_0 varies and the number of such zeroes is odd for all but finitely many values of u_0.

4.2.2. *Connections in the Planar Problem.* The collinear problem is a subsystem of the zero angular momentum planar problem so the connections from triple collision to infinity found above can be viewed as part of the planar problem. In this section, nearby connections from the Lagrangian restpoints to infinity will be constructed. These will be one-parameter families of connecting orbits spiralling around the discrete set of collinear connections.

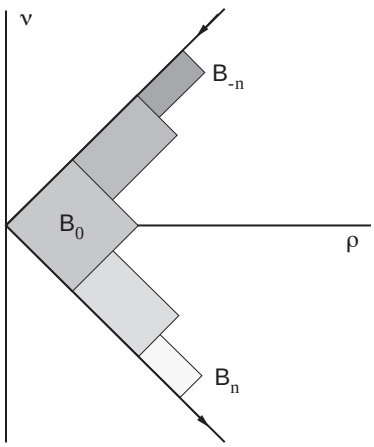

FIGURE 16. Boxes Near Infinity (schematic)

Recall from section 3 that the combination of restpoint connections in the collision manifold between the Lagranagian and Eulerian restpoints and complex eigenvalues at the Eulerian ones had the effect of causing part of $W^u(L_{+,-})$ to form a spiralling manifold around the collinear submanifold converging to $W^u(E_j)$ (see figure 12). We now know that there are transverse intersections of $W^u(E_j)$ and $W^s(\infty)$. Consider a four-dimensional local section to the flow along such a connecting orbit. As in section 3 the implications of spiralling are more easily understood if one introduces polar coordinates around the codimension-two collinear manifold and then consider a three-dimensional half-space of fixed angle. Since $W^s(\infty)$ is of codimension one, coordinates can be chosen so that it appears as a plane transverse to $W^u(E_j)$ which appears as a curve. The intersection of $W^u(L_{+,-})$ with this half-space also appears as a curve, which approaches $W^u(E_j)$ as the angle determining the half-space tends to infinity. This situation is depicted in figure 12. It is obvious from the figure that in each half-space there is a point of transverse intersection of $W^u(L_{+,-})$ and $W^s(\infty)$. Taking all of these point together, one finds that there is a spiralling curve of transverse intersections of $W^u(L_{+,-})$ and $W^s(\infty)$. It is not difficult to prove this from the definition of a spiralling invariant manifold.

Proposition 5. *Let the masses be chosen to satisfy the hypotheses of Propositions 3 and 4. Then in a Poincaré section, every transverse connecting orbit between E_j (or E_j^*) and parabolic infinity is the core of an analytic spiralling curve of transverse connecting orbits between $L_{+,-}$ (or $L_{+,-}^*$) and parabolic infinity.*

4.3. **Boxes Near Infinity.** To complete the proof, it remains to construct four-dimensional boxes near infinity which are linked with the stable and unstable manifolds of the Lagrangian restpoints and which are mapped appropriately across one another while they are near infinity. Easton and McGehee[9], and Robinson [26, 27] describe a construction of boxes having the required mapping properties near infinity. In this section, this construction will be summarized and appropriate modifications will be made to get the linking.

As shown above, a neighborhood of infinity in the Poincaré section is the product of a part of the two-sphere with the (ρ, ν)-plane. Recall that there are coordinates

such that the Poincaré map is given by equations (10). Ignoring $O(5)$ terms, this map is a product of a saddle-like map in the (ρ, ν)-plane and the identity in the two-sphere. For this simplified map, one can construct four-dimensional boxes as products of a fixed box in the two-sphere with a family of boxes in the (ρ, ν)-plane as indicated in figure 16. Even for a product mapping, there are some technicalities arising from the fact that the mapping in the (ρ, ν)-plane is not hyperbolic. However, it is sufficiently similar to the hyperbolic case to push through the construction. In particular, the direction parallel to the stable foliation is contracted and that parallel to the unstable foliation is expanded and there are invariant cone families. Another problem is the lack of stretching in the directions associated to the two-sphere; rather than mapping across one another, the four-dimensional boxes map exactly onto one another in these directions. However, this type of mapping is adequate for the homological symbolic dynamics.

Although the Poincaré map is not a product, Robinson succeeds in constructing these boxes anyway by making use of a continuous invariant foliation which will now be described (see figure 17). This figure depicts the two-sphere and the surface $W^u(L_{+,-})$ as one-dimensional, but otherwise gives a good representation of the situation. As noted already above, the three-dimensional stable and unstable manifolds are foliated into curves of points asymptotic to a given binary orbit in the two-sphere. One would like extend these foliations from the parabolic orbits to the elliptic orbits near infinity. A fundamental domain for the Poincaré map restricted to the unstable manifold can be thickened into a four-dimensional region by appending to each point of the fundamental domain a curve transverse to the unstable manifold extending into the elliptic region. If this is done carefully and extended by iteration of the inverse Poincaré map, an invariant foliation results. This foliation is smooth except possibly on $W^s(\infty)$. By using an invariant cone family argument one can show that the foliation is at least continous on $W^s(\infty) \setminus S^2$ in the sense that as one approaches a point of $W^s(\infty) \setminus S^2$ the fibers converge C^1 to the fibers in $W^s(\infty)$. The argument fails on the two-sphere because the derivative matrix of the mapping (10) is the identity there and so the tangent plane to $W^s(\infty)$ cannot be characterized as the unique plane remaining in a cone family under iteration.

Using this foliation, one can introduce coordinates which make the construction of the boxes more transparent. First replace (ρ, ν) by coordinates (ξ, η) to bring $W^s(\infty)$ to the coordinate plane $\xi = 0$ and $W^u(\infty)$ to the coordinate plane $\eta = 0$. Thus (ξ, z) provide coordinates on $W^u(\infty)$. Next set $(\xi', z') = \pi(\xi, \eta, z)$ where π is projection onto $W^u(\infty)$ along the foliation. Then (ξ', z', η) provide continuous coordinates in a neighborhood of infinity. By invariance of the foliation, these coordinates have the property that z' is invariant under iteration of the Poincaré map. In this way the drift in the S^2 directions can be controlled.

With these coordinates, the construction of the boxes proceeds almost as in the case of a product map. An arbitrary box can be chosen in the two-sphere. The set of all points in the unstable manifold which project to this box can be thickened into a four-dimensional slab, $0 \leq \eta \leq \delta$, over the unstable manifold and then the boxes $B_{-n}, \ldots, B_0, \ldots, B_n$ are constructed by iterating this slab under the inverse Poincaré map as indicated schematically in figure 16 (see [26] for move details).

To use this construction here it is necessary to choose an appropriate box in the two-sphere. It has been shown above that the stable and unstable manifolds of

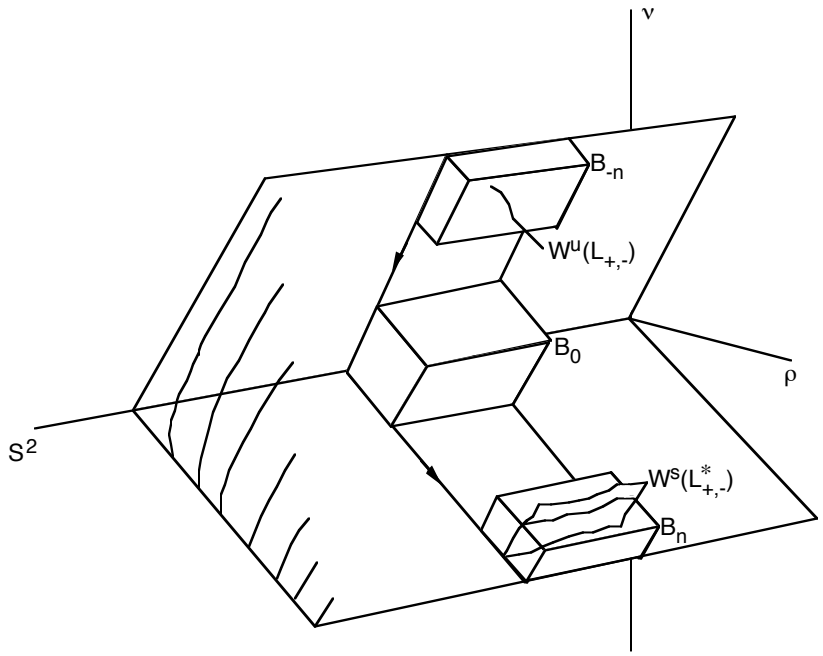

FIGURE 17. Linking of Boxes Near Infinity

the Lagrangian restpoints intersect the stable and unstable manifolds of parabolic infinity in spiralling curves. Projecting these to the orbit two-sphere yields analytic spiralling curves converging to the collinear two-body orbit as shown in figure 18. Since the spiral associated to the stable manifold of the Lagrangian restpoint spirals in the opposite sense from that associated to the unstable manifold, there will be infinitely many finite-order crossings. Therefore it is possible to construct a two-dimensional box in the two-sphere as indicated in the figure.

Next it is necessary to assure that the boxes B_{-n} and B_n are linked with the incoming unstable manifold and outgoing stable manifold of triple collision, respectively, as indicated in figure 17. Consider B_{-n}, the box which is intended to link the incoming unstable manifold of triple collision; the other case is easier. This box is part of a preimage of the original four-dimensional slab of thickness δ. This slab is foliated into smooth three-dimensional manifolds of the form $\xi' = c$. Using another invariant cone family argument, one can show that under inverse iteration, these manifolds converge C^1 to $W^s(\infty)$ at least away from the two-sphere. Hence B_{-n} can be decomposed into smooth, continously varying three-dimensional slices parametrized by c. Now consider the slice $c = 0$, that is, $W^s(\infty) \cap B_{-n}$ (see figure 19). The top and bottom surfaces are smooth preimages of the top of the original slab. The sides are determined by the choice of the box in S^2. If the latter box is sufficiently small then, as indicated in the figure, $W^u(L_{+,-}) \cap W^s(\infty)$ exits the box on the sides rather than on the top or bottom. Since $W^u(L_{+,-})$ is a two-dimensional manifold transverse to $W^s(\infty)$ and since the slices into which B_{-n} has been decomposed are C^1 close to $W^s(\infty)$, the slices of $W^u(L_{+,-})$ are smooth curves

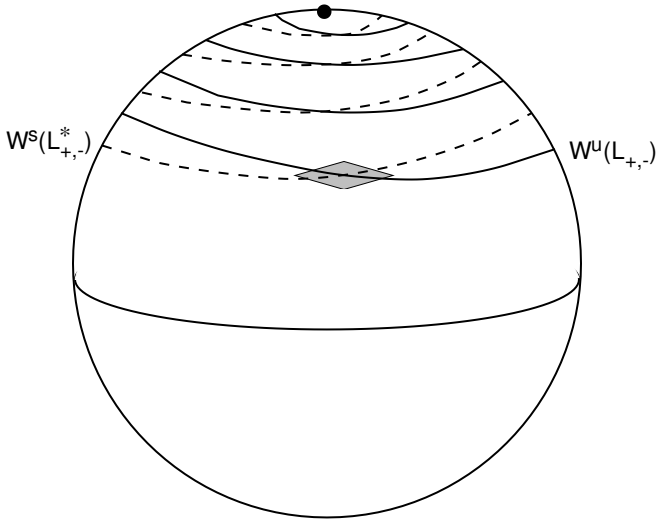

FIGURE 18. Projection of Orbits Heteroclinic Between Collision and Infinity

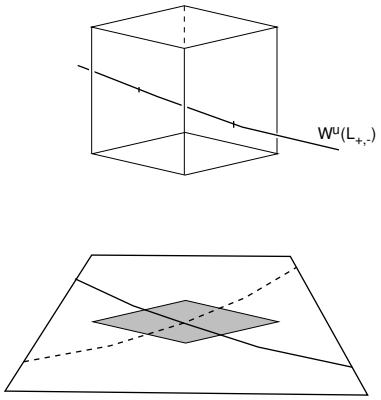

FIGURE 19. Linking of B_{-n} with $W^u(L_{+,-})$ Inside $W^s(\infty)$

depending continously on c. It follows that $W^u(L_{+,-})$ in B_{-n} is homeomorphic to the product of figure 19 with an interval. Hence B_{-n} is linked in the desired way with $W^u(L_{+,-})$.

Finally, for the purposes of connecting the dynamics at infinity with the invariant set near collision it is necessary to replace B_{-n} by a smaller box which can be followed back to a neighborhood of $L_{+,-}$. The choice of the box in the two-sphere controls the size of B_{-n} in the z' directions and B_{-n} can be made thin in the ξ'-direction by choosing a small δ. It remains to shrink the box in the η-direction.

Because of the transversality of the intersection $W^s(\infty) \cap W^u(L_{+,-})$ and the fact that the fibers in B_{-n} are near to the fibers in $W^s(\infty)$ each fiber in B_{-n} intersects $W^u(L_{+,-})$ at most once. In other words, $W^u(L_{+,-}) \cap B_{-n}$ is a graph over its projection to $W^u(\infty)$. Extending this graph to a graph, $\eta = f(\xi', z)$, over the projection of B_{-n} to $W^u(\infty)$ and then thickening it slightly to $\{|\eta - f(\xi', z)| \leq \epsilon\}$ produces a four-dimensional box which is small and is still linked with $W^u(L_{+,-})$. If the inclusion of this smaller box into the old box B_{-n} is viewed as a trivial Poincaré map, it satisfies the homological conditions necessary to incorporate it into the symbolic dynamics. This completes the construction of all of the four-dimensional boxes and the proof of the theorem.

References

[1] V. M. Alexeev. Quasirandom dynamical systems i. *Math. USSR-Sb.*, 5:73–128, 1968.

[2] V. M. Alexeev. Quasirandom dynamical systems ii. *Math. USSR-Sb.*, 6:505–560, 1968.

[3] V. M. Alexeev. Quasirandom dynamical systems iii. *Math. USSR-Sb.*, 7:1–43, 1969.

[4] R. Devaney. Structural stability of homothetic solutions of the collinear n-body problem. *Cel. Mech.*, 19:391–404, 1979.

[5] R. Devaney. Triple collision in the planar isosceles 3-body problem. *Inv. Math.*, 60:249–267, 1980.

[6] R. Devaney. Singularities in classical mechanical systems. In A. Katok, editor, *Ergodic Theory and Dynamical Systems I, Proceedings–Special Year, Maryland 1979–1980*, pages 211–333. Birkhauser, Boston, 1981.

[7] R. Easton. Parabolic orbits for the planar three body problem. *JDE*, 52:116–134, 1984.

[8] R. Easton. Capture orbits and Melnikov integrals in the planar 3-body problem. 1990.

[9] R. Easton and R. McGehee. Homoclinic phenomena for orbits doubly asymptotic to an invariant three-sphere. *Ind. Jour. Math.*, 28:211–240, 1979.

[10] L. Euler. De motu rectilineo trium corporum se mutuo attahentium. *Novi Comm. Acad. Sci. Imp. Petrop.*, 11:144–151, 1767.

[11] J. M. Irigoyen. La variété de collision triple dans le cas isoscèle du problème des trois corps. *C. R. Acad. Sci. Paris*, 290:B489–B492, 1980.

[12] E. Lacomba and L. Losco. Triple collision in the isosceles three-body problem. *Bull. Amer. Math. Soc.*, 3:710–714, 1980.

[13] J. L. Lagrange. *Ouvres, vol.6*. Gauthier-Villars, Paris, 1873.

[14] J. Llibre and C. Simó. Some homoclinic phenomena in the three-body problem. *JDE*, 37, 3:444–465, 1980.

[15] R. McGehee. A stable manifold theorem for degenerate fixed points with applications to celestial mechanics. *JDE*, 14:70–88, 1973.

[16] R. McGehee. Triple collision in the collinear three body problem. *Inv. Math.*, 27:191–227, 1974.

[17] R. McGehee. Singularities in classical celestial mechanics. In *Proc. of Int. Cong. Math., Helsinki*, pages 827–834, 1978.

[18] R. Moeckel. Orbits of the three-body problem which pass infinitely close to triple collision. *Amer. Jour. Math*, 103,6:1323–1341, 1981.

[19] R. Moeckel. Orbits near triple collision in the three-body problem. *Ind. Jour. of Math.*, 32:221–239, 1983.

[20] R. Moeckel. Heteroclinic phenomena in the isosceles three-body problem. *SIAM Jour. Math. Anal.*, 15:857–876, 1984.

[21] R. Moeckel. Spiralling invariant manifolds. *Jour. Diff. Eq.*, 66:189–207, 1984.

[22] R. Moeckel. Chaotic dynamics near triple collision. *Arch. Rat. Mech*, 107,1:37–69, 1989.

[23] J. Moser. Regularization of Kepler's problem and the averaging method on a manifold. *Comm.Pure Appl.Math*, 23:609–636, 1970.

[24] J. Moser. *Stable and Random Motions in Dynamical Systems*, volume 77 of *Annals of Math. Studies*. Princeton Univ. Press, Princeton, 1973.

[25] J. Quillen. *An application of the Melnikov method to the planar problem*. PhD thesis, Univ. of Colorodo, 1986.

[26] C. Robinson. Homoclinic orbits and oscillation for the planar three-body problem. *JDE*, 52, 3:356–377, 1984.
[27] C. Robinson. Stable manifolds in hamiltonian systems. In K. Meyer and D. Saari, editors, *Proceedings of the AMS Summer Research Conference on Hamiltonian Systems*, volume 81 of *Contemporary Mathematics*, pages 77–98, Providence, 1987. AMS.
[28] C. Robinson and D. Saari. N-body spatial parabolic orbits asymptotic to collinear central configurations. *JDE*, 48:434–459, 1983.
[29] C. Siegel and J. Moser. *Lectures on Celestial Mechanics*. Springer-Verlag, New York, 1971.
[30] C. L. Siegel. Der Dreierstos. *Ann.Math.*, 42:127–168, 1941.
[31] C. Simó. *Analysis of triple collision in the isosceles problem*, pages 203–224. Marcel Dekker, 1981.
[32] K. Sitnikov. Existence of oscillating motions for the three body problem. *Dokl. Akad. Nauk USSR*, 133, 2:303–306, 1960.
[33] K. F. Sundman. Nouvelles recherches sur le problèm des trois corps. *Acta Soc. Sci. Fenn*, 35:1–27, 1909.
[34] Z. Xia. Melnikov method and transversal homoclinic points in the restricted three-body problem. *JDE*, 96,1:170–184, 1992.
[35] Z. Xia. Arnold diffusion and oscillatory solutions in the planar three-body problem. *JDE*, 110:289–321, 1994.

School of Mathematics, University of Minnesota, Minneapolis MN 55455
E-mail address: rick@math.umn.edu